Sedimentation of colloidal nanoparticles in fluids: efficient and robust numerical evaluation of analytic solutions of the Mason-Weaver equation

Lancelot Barthe, Martinus H. V. Werts

Sedimentation of colloidal nanoparticles in fluids: efficient and robust numerical evaluation of analytic solutions of the Mason-Weaver equation

Lancelot Barthe and Martinus H. V. Werts*
Univ Rennes, CNRS, SATIE – UMR8029, F-35000 Rennes, France and
École normale supérieure de Rennes, Department of Engineering Sciences,
Lab. SATIE, Campus de Ker Lann, F-35170 Bruz, France
(Dated: December 16, 2022)

The Mason-Weaver equation (MWE) is an advection-diffusion equation that describes the time-evolution of the concentration profile of a solution of nanoparticles undergoing sedimentation and Brownian motion from an initially homogeneous state towards sedimentation equilibrium. In spite of the availability of analytic solutions, recent work has used numerical schemes to obtain practical solutions for the MWE. Here, the numerical evaluation of analytic solutions of the MWE is investigated using standard floating-point computations. It was found that the numerical evaluation is not always straightforward as this involves summing over an infinite series of terms which is sometimes automatically truncated due to limitations in floating-point computation. By combining several analytic expressions, each having its own range of validity in the MWE parameter space, robust and computationally efficient numerical evaluation of the solution is finally achieved. The expressions and the numerical procedure have been coded into a computer program enabling practical calculation of nanoparticle sedimentation profiles.

I. INTRODUCTION

The development of synthetic functional nanoparticles for applications in medicine, solar energy and so forth has brought renewed interest in the sedimentation behaviour of such small particles dispersed in fluids (*i.e.* colloidal solutions[1]). The sedimentation behaviour of sufficiently small colloidal particles is governed both by sedimentation (which forces the particles in a specific direction, typically towards the bottom of the container) and diffusion (which tends to disperse the particles through the entire available volume). The basic model describing this behaviour was established almost a century ago in the form of a partial differential equation now known as the Mason-Weaver equation (MWE)[2].

In their original publication, Mason and Weaver (M&W) gave an analytic solution for their equation. This solution takes the form of a periodic infinite series (*i.e.* a Fourier series) that converges slowly to the true solution, in particular at short times, requiring summation of many terms of the series to overcome the oscillatory behaviour known as the Gibbs phenomenon. More anecdotally, there are typographical errors in some of the formulae in the original paper, which does not facilitate the task of coding the expressions into a working computer program. It may be for these reasons that recent work has resorted to using finite-difference schemes to calculate numerical solutions for the MWE[3][4]. These finite-difference schemes are computationally inexpensive for short times, and may also be adapted to cases that deviate from the classic MWE (*e.g.* different initial conditions, non-constant diffusion and sedimentation coefficients). However, finite-difference schemes do not generally conserve the total mass in the system, may display unphysical numerical divergence at very long times, and become expensive for calculation of the solution at long times.

Therefore, it is desirable to have an efficient method for evaluating the analytic solution that exists. The analytic solution holds for all times, will not display deviations from mass conservation, and its computation is likely to be inexpensive even for longer times. Very recently, Holt *et al.* used the analytic solution in their work on the rôle of nanoparticle sedimentation in cytotoxicity studies.[5] They reported that they needed to numerically sum a great number of terms (over 10^5) in the expression by M&W to obtain satisfactory results, but did not give further details. Here, the numerical evaluation of the expressions derived by Mason & Weaver is further investigated over a wide range of parameters.

In addition to the infinite-series solution (ISS) requiring computation of many terms, M&W derived an integral solution (IntS) that works for short times and does not involve summation over an infinite series. On basis of the original work, further expressions can be derived for the case where sedimentation begins to dominate over the Brownian diffusion term, *i.e.* at high Péclet numbers (hiPe). We found that, with current 'double precision' floating-point arithmetic and scientific software libraries, each of these three solutions has its own range of parameters where it produces reliable results. The standard numerical floating-point precision of 64 bits was used. In certain critical cases, 80 bits 'extended precision' was tested, but this did not substantially improve the numerical results. In contrast, switching to 32 bits 'single precision' floating point proved highly detrimental to numerical evaluation of the expressions.

A computer code was developed for numerical evaluation the different analytic solutions of the MWE in its dimensionless form. The program also provides a function that automatically selects evaluation of the relevant

* Correspondence to: martinus.werts@ens-rennes.fr

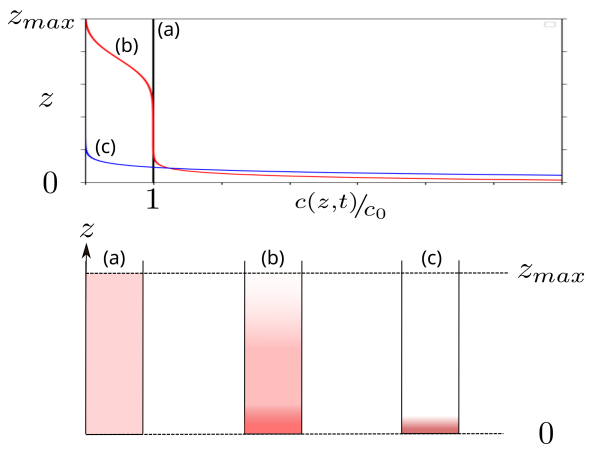

Figure 1. Sedimentation behaviour of Brownian particles as described by the Mason-Weaver equation (MWE). The particles are initially homogeneously distributed. Top: concentration profiles as a function of height at (a) $t = 0$, (b) intermediate t, and (c) sedimentation equilibrium ($t \to \infty$, steady-state solution of the MWE). Bottom: visualization of the corresponding vertical gradients such as can be observed, e.g. with gold nanoparticles in solution.[4]. The z coordinates refer to the 'real-world' dimensional version of the MWE, where $z = 0$ is the bottom of the cell. The y coordinates in the dimensionless form move in the opposite direction, $y = 0$ being the top of the cell.

expression on basis of the input parameters, and a function that handles the interface between the 'real world' parameters and the dimensionless expressions. The latter can readily and transparently be used to calculate concentration profiles for Brownian nanoparticles undergoing sedimentation in solution.

II. THE MASON-WEAVER EQUATION

With concentration c, position z and time t, the time-evolution of the nanoparticle concentration profile $c = c(z,t)$ of a colloidal solution undergoing sedimentation is illustrated in Figure 1, from an initially homogeneous distribution of nanoparticles to an equilibrium nanoparticle gradient. This evolution is governed by the MWE, Eqn. (1).

$$\frac{\partial c}{\partial t} = D\frac{\partial^2 c}{\partial z^2} + sg\frac{\partial c}{\partial z} \tag{1}$$

which has boundary conditions

$$D\frac{\partial c}{\partial z} + sgc = 0 \quad @(z = 0, z = z_{max}) \tag{2}$$

and initial condition

$$c(z, t = 0) = c_0 \tag{3}$$

D, s and g are, respectively, the diffusion coefficient of the particles in the fluid, their sedimentation coefficient and the gravitational acceleration. The z-axis corresponds to the height position in the cell, with $z = 0$ being the bottom and $z = z_{\max}$ the top.

A dimensionless form of the Mason-Weaver equation is obtained through application of the changes of variable expressed in Eqn. (4).

$$\begin{aligned} z_0 &= \frac{D}{sg} \qquad \alpha = \frac{z_0}{z_{\max}} \qquad t_{\text{sed}} = \frac{z_{\max}}{sg} \\ \tau &= \frac{t}{t_{\text{sed}}} \qquad y = 1 - \frac{z}{z_{\max}} \end{aligned} \tag{4}$$

The dimensionless form of the MWE for $c = c(y,\tau)$ is then given by Eqns. (5)-(7).

$$\frac{\partial c}{\partial \tau} = \alpha\frac{\partial^2 c}{\partial y^2} - \frac{\partial c}{\partial y} \tag{5}$$

$$\alpha\frac{\partial c}{\partial y} - c = 0 \qquad @(y = 0, y = 1) \tag{6}$$

$$c(y, \tau = 0) = c_0 \tag{7}$$

III. INFINITE-SERIES SOLUTION (ISS)

M&W showed that Eqn. (8) is a solution to the dimensionless form of the MWE, Eqn. (5).[2]

$$\begin{aligned} \frac{c(y,\tau)}{c_0}\bigg|_{\text{ISS}} &= \frac{\exp\left(\frac{y}{\alpha}\right)}{\alpha\left(\exp\left(\frac{1}{\alpha}\right) - 1\right)} + \\ 16\alpha^2\pi\exp\left(\frac{2y-\tau}{4\alpha}\right)\sum_{m=1}^{\infty}\frac{\exp\left(-\alpha m^2\pi^2\tau\right)m}{(1+4\pi^2m^2\alpha^2)^2}&\left(1-(-1)^m\exp\left(\frac{-1}{2\alpha}\right)\right)\left(\sin\left(m\pi y\right)+2\pi m\alpha\cos\left(m\pi y\right)\right) \end{aligned} \tag{8}$$

The first term of this 'infinite series' solution (ISS) corresponds to the steady-state solution, $c_{ss}(y)$, while the second term (*i.e.* the infinite series) corresponds to the transient solution, $c_t(y,\tau)$. This is expressed as Eqn. (9).

$$\frac{c(y,\tau)}{c_0} = c_{ss}(y) + c_t(y,\tau) \tag{9}$$

Taking the limit of the complete solution when τ tends towards infinity yields the steady-state solution, since the transient solution vanishes at long times (Eqn. (10)).

$$\lim_{\tau\to\infty}\left[\frac{c(y,\tau)}{c_0}\right] = c_{ss}(y) \tag{10}$$

The transient term of the solution has the following form (Eqn. (11)).

$$c_t(y,\tau) = s_f(y,\tau)\sum_{m=1}^{\infty} s_m(y,\tau) \tag{11}$$

where $s_m(y,\tau)$ and $s_f(y,\tau)$ are, respectively, the terms of the series and a constant pre-factor with respect to m that can be taken out of the summation.

As pointed out earlier,[2][5][6] the series converges rapidly for large values of $\{\tau,\alpha\}$, but slowly for small values. A large number of terms for the series (*e.g.*, >100000) might be evaluated and added to the final result in the hope of reaching convergence, as was done by Holt *et al.*[5]. However, it was found in the present work using standard double precision floating-point arithmetic that the factor $\frac{\exp(-\alpha m^2\pi^2\tau)m}{(1+4\pi^2m^2\alpha^2)^2}$ in the series summation of (8), numerically evaluates as strictly zero already for modest values of m. Any terms evaluated beyond that point do not contribute numerically to the solution, leading to a false convergence. Switching from the standard 64-bit to 80-bit floating-point precision did not substantially alleviate this problem.

This numerical artefact limits the number of terms that can be usefully evaluated for the ISS. It also provides a clear condition for stopping evaluation of the series: the loop evaluating terms for increasing m can be ended once $\frac{\exp(-\alpha m^2\pi^2\tau)m}{(1+4\pi^2m^2\alpha^2)^2}$ numerically evaluates to zero. The result obtained in this manner is the best result numerically attainable, which does not necessarily mean that that result is sufficiently close to the correct solution.

Satisfactory results with the numerical evaluation of the ISS are obtained systematically only for $\alpha \geqslant 0.02$. For $\alpha < 0.02$, significant high-frequency numerical oscillations are often present in the 'best' numerically attainable result, in particular at low values for τ (short times). It is numerically impossible to add further terms. Low values of α correspond to high Péclet numbers, where sedimentation dominates diffusion giving rise to a sharp sedimentation front, requiring a large number high frequency terms to be included.

The limits for α and τ for correct evaluation of the ISS were investigated in more detail, and it was found possible to work at values for α slightly lower than 0.02 (say, 0.01), but only for values for larger values of τ (say, 0.5). It is possible to automatically detect numerical artefacts in evaluated ISS concentration profiles, by testing if the result is monotonous (within a certain tolerance) and by detecting deviations is the mass conservation. This may identify satisfactory numerical evaluations of the ISS at $\alpha < 0.02$. However, the safe choice was made finally to constrain validity of the numerically evaluated ISS to $\alpha \geqslant 0.02$. At $\alpha < 0.02$, other analytic expressions exist that have better numerical behaviour, not needing any summing over a series (see the "high Péclet" solution below).

Under the constraint that $\alpha \geqslant 0.02$ and using the aforementioned numerical vanishing of the factor $\frac{\exp(-\alpha m^2\pi^2\tau)m}{(1+4\pi^2m^2\alpha^2)^2}$ as a stopping condition, the number of terms of the series that is included in the numerical evaluation of the ISS is plotted as a function of τ for various values of α in Figure 2. This graph clearly illustrates the strong increase in number of terms for low α,τ. This makes evaluation of the ISS in those cases computationally expensive. The number of terms reaches almost 2000 for $\alpha = 0.02$ and $\tau = 0.001$, but drops rapidly as diffusion starts dominating sedimentation and when solutions close to the steady-state are evaluated.

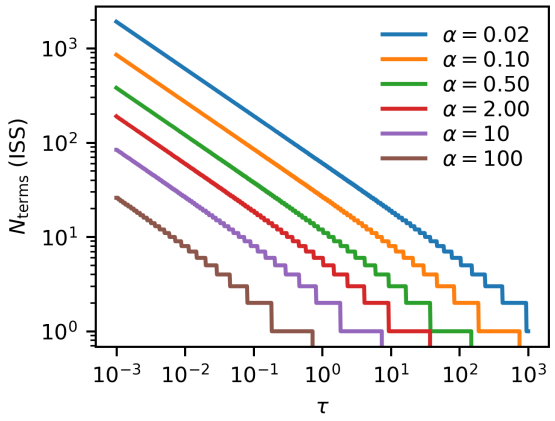

Figure 2. The number of terms, N_{terms}, used in evaluation of the ISS as a function of τ for different values of α ($\geqslant 0.02$). Inclusion of further terms is not possible due to very small factors numerically evaluating as zero in floating-point arithmetic (see Text).

IV. INTEGRAL SOLUTION (INTS) FOR SMALL $\{\alpha,\tau\}$

At small $\{\alpha,\tau\}$, where a large number of terms need to be included for evaluation of the ISS, M&W suggested[2]

an alternative solution that they obtained using the image method. This approximate analytic solution will be referred to as the 'integral' solution (IntS, Eqn. (12)). It is highly accurate at very small values of $\{\alpha, \tau\}$, as is clear from the very low RMS error between IntS and ISS.

$$\begin{aligned}
\left.\frac{c(y,\tau)}{c_0}\right|_{\text{IntS}} = \\
\frac{1}{2}\exp\left(\frac{y-1}{\alpha}\right)\left[1+\frac{y+\tau-1}{\alpha}\right]\left[\theta\left(\frac{2-y-\tau}{\sqrt{4\alpha\tau}}\right)-\theta\left(\frac{1-y-\tau}{\sqrt{4\alpha\tau}}\right)\right] \\
-\sqrt{\frac{\tau}{\alpha\pi}}\exp\left(\frac{y-1}{\alpha}\right)\left[\exp\left(-\left(\frac{2-y-\tau}{\sqrt{4\alpha\tau}}\right)^2\right)-\exp\left(-\left(\frac{1-y-\tau}{\sqrt{4\alpha\tau}}\right)^2\right)\right] \\
+\frac{1}{2}\exp\left(\frac{y}{\alpha}\right)\left[1+\frac{y+\tau}{\alpha}\right]\left[\theta\left(\frac{1+y+\tau}{\sqrt{4\alpha\tau}}\right)-\theta\left(\frac{y+\tau}{\sqrt{4\alpha\tau}}\right)\right] \\
+\sqrt{\frac{\tau}{\alpha\pi}}\exp\left(\frac{y}{\alpha}\right)\left[\exp\left(-\left(\frac{1+y+\tau}{\sqrt{4\alpha\tau}}\right)^2\right)-\exp\left(-\left(\frac{\tau+y}{\sqrt{4\alpha\tau}}\right)^2\right)\right] \\
+\frac{1}{2}\left[\theta\left(\frac{1-y+\tau}{\sqrt{4\alpha\tau}}\right)-\theta\left(\frac{\tau-y}{\sqrt{4\alpha\tau}}\right)\right]
\end{aligned} \tag{12}$$

Using the same symbol as M&W, $\theta(x) = (2/\sqrt{\pi})\int_0^x \exp(-t^2)\,\mathrm{d}t$ is the error function, $\mathrm{erf}(x)$.

IntS becomes less accurate at larger values, and fails badly when used outside of its domain of validity. For instance, the IntS exhibits convergence issues when $\alpha < 0.02$ due to the limited stiffness of the error function at the junction (*i.e* anti-symmetry points) in the construction process by mirror image. Thus, both ISS and IntS cannot be used for $\alpha < 0.02$.

In practice, the principal advantage of the IntS is the reduction of the computational effort compared to ISS. The range of values $\{\alpha, \tau\}$ where the IntS is favourably applied instead of the ISS can be found by considering the mean square error (MSE), calculated between the IntS and the ISS, and identifying where this MSE is very small. Subsequently, a function $\tau_{switch}(\alpha)$ should be found in the aim of giving the time τ value below which the IntS will be used instead of the ISS, while remaining below a given MSE. The MSE of IntS relative to ISS is calculated over a grid spanning a range of α and τ. Visualized as a 'heat map' (Figure 3) it is clearly seen that there is a region at low $\{\alpha, \tau\}$ where the MSE is very small, and where IntS can be used instead of ISS in order to limit the computation effort.

Using curve fitting, a parametric function $\tau_{switch}(\alpha)$ was obtained that defines a boundary for the region where IntS has low MSE (typically, less than 10^{-8}). The function is given by Eqn. (13), and is traced in red in Figure 3). Below the red trace, the IntS is used. Above the trace, the ISS is used. The range of α for which this τ_{switch} is considered has been chosen to go from 0.02 to 20.

$$\tau_{switch}(\alpha) = \begin{cases} A_1\alpha^{k_1} & \text{if } \alpha < 0.04625 \\ A_2\alpha^{k_2} & \text{else} \end{cases} \tag{13}$$

where A_i, k_i are the constants given in Eqn. (14).

$$\begin{aligned} A_1 = 8.134 \quad k_1 = 0.9666 \\ A_2 = 0.02934 \quad k_2 = -0.8634 \end{aligned} \tag{14}$$

This parametrization was made on a specific computer system (Intel Core i7 (12th gen.) processor, Python 3.9.13 with numpy 1.22.3, scipy 1.9.1), and might depend somewhat on the numerical properties of the specific system, *e.g.* the software implementation for the evaluation of the error function $\theta(x)$. The optimal parameters for defining the switch between IntS and ISS are not expected to change significantly for other computer systems and languages (Matlab, FORTRAN), since these use the same basic numerical libraries and floating-point operations.

As illustrated in Figure 4, IntS is roughly between 50 to 10000 times faster than ISS, while having a MSE relative to ISS of less than 10^{-8}. This is a useful gain in performance, especially in cases where multiple evaluations of profiles need to be made, such as in iterative curve fitting. The Figure also shows the switching between IntS and ISS at τ_{switch}, after which only the ISS is considered (MSE becomes trivially 0). Taking the decision on which solution (IntS or ISS) to use generates negligible overhead.

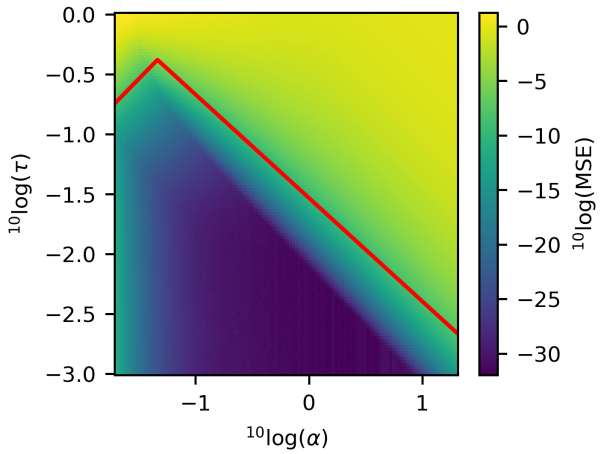

Figure 3. Logarithm of the MSE between the IntS and ISS (color map) as a function of α and τ (plotted as their logarithms). The red trace is the boundary defined by τ_{switch} in Eqn. (13).

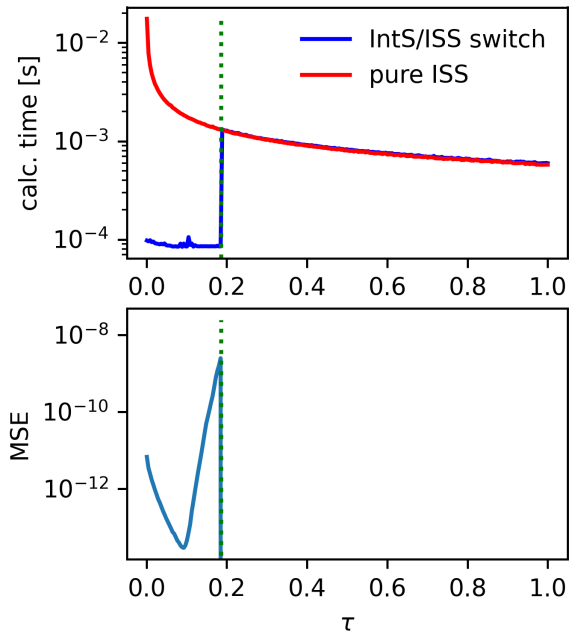

Figure 4. Comparison of pure ISS and mixed IntS/ISS for the calculation of MW concentration profiles at $\alpha = 0.02$ as a function of τ. Top: Calculation time for a single profile. Bottom: Mean-square error between IntS/ISS and ISS solutions, dropping to zero when ISS is used in both calculations. Profiles were calculated over y from 0 to 1 in 200 points. The calculation time was measured for the Python program executed on a single core of an Intel Core i7 (12th gen.) 64-bit processor running at 2.4 GHz. The green dotted vertical line indicates where the switch between IntS and ISS is made.

V. APPROXIMATE "HIGH PÉCLET" SOLUTIONS FOR VERY SMALL α

For very small α ($\alpha < 0.02$, as explained above), neither the IntS nor the ISS can be reliably evaluated numerically. This is illustrated in Figure 5 which presents a typical case where both IntS and ISS display numerical artefacts. The case shown is for $\{\alpha = 0.01, \tau = 0.23\}$, but many combinations of parameters yield this kind of artefacts when $\alpha < 0.02$, indicating the need for an alternative solution for small α.

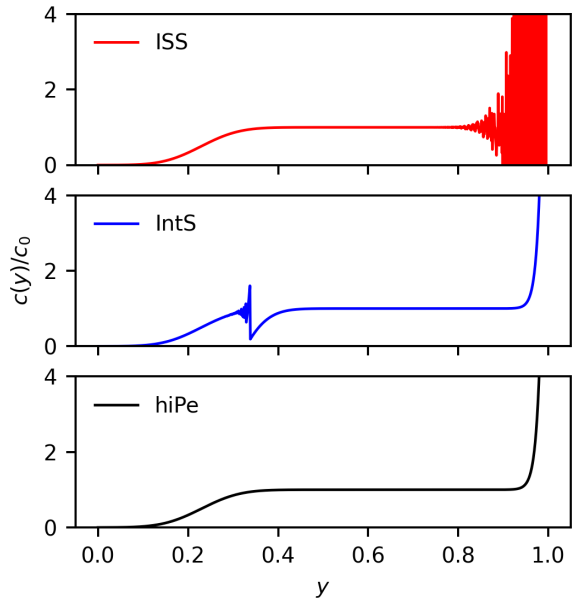

Figure 5. Example of the failure of both ISS and IntS, when $\alpha < 0.02$. Three analytic solutions to the Mason-Weaver were evaluated for $\{\alpha = 0.01, \tau = 0.23\}$. Only the hiPe solution gives a completely artefact-free concentration profile.

The situation where α is small corresponds to a high Péclet number, *i.e.* the contribution of nanoparticle diffusion becomes small compared to the sedimentation. The particles sediment with a clear sedimentation front that shows only little diffusive broadening. The advection due to sedimentation and the diffusive behaviour can be decoupled which leads to an approximate solution in the form of Eqn. (15), referred as "high Péclet" (hiPe) solution.

$$\left.\frac{c(y,\tau)}{c_0}\right|_{\text{hiPe}} = \frac{1}{2}\left[1 + \theta\left(\frac{y-\tau}{\sqrt{4\alpha\tau}}\right) + K(\tau)\frac{\exp\left(\frac{y}{\alpha}\right)}{\alpha\left(\exp\left(\frac{1}{\alpha}\right) - 1\right)}\right] \tag{15}$$

In Eqn. (15), $K(\tau)$ corresponds to a mixing between the steady state and the propagating diffusive front solutions. $K(\tau)$ was obtained using mass conservation con-

sideration (*i.e.* $\int_{y=0}^{y=1} \frac{c(y,\tau)}{c_0} dy = 1$) as proposed in Eqn. (16).

$$K(\tau) = 1 - \sqrt{\frac{4\alpha\tau}{\pi}} \left[\exp\left(\frac{-(\tau-1)^2}{4\alpha\tau}\right) - \exp\left(\frac{-\tau}{4\alpha}\right) \right] + (\tau - 1)\theta\left(\frac{1-\tau}{\sqrt{4\alpha\tau}}\right) + \tau\theta\left(\frac{\tau}{\sqrt{4\alpha\tau}}\right) \quad (16)$$

This "hiPe" solution was found to work well, numerically, for $0.0015 \leqslant \alpha < 0.02$.

For $\alpha < 0.0015$, Eqn. (15) can be modified keeping only the sedimentation front and excluding the steady-state part by limiting the range of y to 0.99. This "hiPe2" solution, Eqn (17), does not conserve mass, and basically only describes the moving sedimentation front, which undergoes a minor broadening due to diffusion. For these very small values of α, the MWE is less relevant, since these systems are almost purely sedimentation systems, with a sharp sedimentation front. We include the "hiPe2" solution so that the entire range of α can be handled.

$$\left.\frac{c(y,\tau)}{c_0}\right|_{\text{hiPe2}} = \frac{1}{2}\left[1 + \theta\left(\frac{y-\tau}{\sqrt{4\alpha\tau}}\right)\right], \quad 0 < y < 0.99 \quad (17)$$

VI. COMBINED, PIECE-WISE ANALYTIC SOLUTION (PWS) FOR SUCCESSFUL NUMERICAL EVALUATION AT ANY α, τ

Considering the different regions in the $\{\alpha, \tau\}$ plane where each of the analytic solutions to the MWE (ISS, IntS, hiPe, hiPe2) can be successfully evaluated numerically, a piece-wise analytic solution (PWS) can be constructed that covers the entire parameter space for $\alpha > 0$ and $\tau > 0$. Figure 6 contains a plot of the domains of application for the different analytic solutions discussed.

The PWS can be formulated according to Eqn. (18), with the understanding that $\alpha > 0$ and $\tau > 0$.

$$\frac{c(y,\tau)}{c_0} = \begin{cases} c_{\text{hiPe2}}(y,\tau,\alpha) & \text{if } \alpha < 0.0015 \\ c_{\text{hiPe}}(y,\tau,\alpha) & \text{if } 0.0015 \leqslant \alpha < 0.02 \\ c_{\text{IntS}}(y,\tau,\alpha) & \text{if } 0.02 \leqslant \alpha < 20 \text{ and } \tau < \tau_{\text{switch}}(\alpha) \\ c_{\text{ISS}}(y,\tau,\alpha) & \text{if } 0.02 \leqslant \alpha < 20 \text{ and } \tau \geqslant \tau_{\text{switch}}(\alpha) \\ c_{\text{ISS}}(y,\tau,\alpha) & \text{if } \alpha \geqslant 20 \end{cases} \quad (18)$$

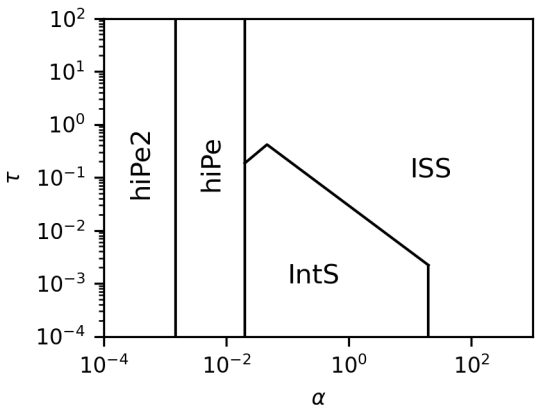

Figure 6. Graph representing the range of application of each numerically evaluated analytic solution to the MWE as a function of $\{\tau, \alpha\}$ in the combined PWS. Evaluation using standard floating-point arithmetic with 64 bits precision.

Eqn. 18 forms the point of entry to the computer program module masonweaver_analytic [7] implementing the computational strategy for evaluation of the analytic solution of the MWE explained in this work. It was coded in the Python programming language[8] with use of the numpy [9] and scipy [10] scientific libraries, and may be readily ported to other languages. The dimensionless Eqn. 18 is implemented as the function routine MW_adim(y, τ, α) which returns a vector[1] containing the numerical values of the nanoparticle concentration profile for the (dimensionless) positions given by the vector y.

Finally, a 'real-world' (dimensional) function routine MW_c_profile(t, $z_{\max}$, D, sg, ...) is provided. It returns a pair of vectors (z, c) giving the numerical values for the (dimensional) positions and corresponding concentrations reproducing the full nanoparticle concentration profile using the analytic solutions of the MWE.

VII. COMPARISON WITH CURVES PUBLISHED BY MASON & WEAVER AND EXPERIMENTAL DATA

In addition to extensive testing of the PWS against the numerical solutions generated by the previously published finite-difference program,[4] the computational accuracy of the combined piece-wise solution was demonstrated by comparing its results to curves from the original publication by M&W.[2]. To this end, these curves were digitized using the Engauge Digitizer software package,[11] converting them into sets of data points representing $c(y,\tau)/c_0$ as a function of y for different values of τ. These curves are shown in Figure 7, together

[1] In this text, a 'vector' is a one-dimensional array of floating-point numbers.

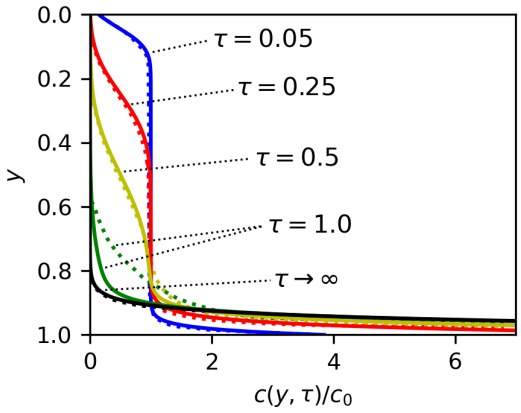

Figure 7. Comparison of the curves from first Figure in the paper by M&W [2] (dotted lines) and the numerically evaluated analytic solution from the present work (continuous lines) for $\alpha = 0.025$.

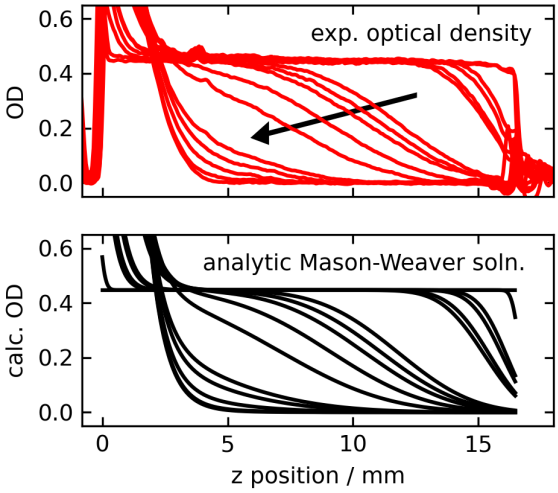

Figure 8. Evolution of the vertical particle density gradient in an aqueous solution of 40 nm diameter gold nanospheres toward sedimentation equilibrium, observed using quantitative digital photography at 277 K. Photos were taken at $t = 0$, 1 h, 21 h, 27 h, 44 h, 52 h, 7 d, 9 d, 11 d, 14 d, 21 d, 23 d, 28 d, 35 d, and 39 d. Top: Experimental optical density profiles obtained from digital photographs.[4] The arrow indicates the direction of time. Bottom: theoretical optical density (concentration) profiles evaluated using the analytic solution of the Mason-Weaver equation, with $D = 5.1 \times 10^{-12}\,\mathrm{m^2 s^{-1}}$ and $s = 7.9 \times 10^{-10}\,\mathrm{s}$.

with curves obtained using the numerical evaluation of the PWS by our computer program.

It is evident from Figure 7 that the curves evaluated by our PWS procedure are in accordance with the curves from the original publication. No precise error estimation is proposed here, since the digitization process by itself is a source of significant uncertainty. Interestingly, the PWS result for $\tau = 1$, does not match the original M&W curves. This is a minor mistake in the original publication.

The numerically evaluated analytic solution also fits previously published experimental sedimentation profiles obtained using quantitative digital photography of gold nanoparticles in aqueous solution undergoing sedimentation.[4] This is shown in Figure 8 which revisits Figure 2 from the original publication, using the analytic solution instead of the numerical finite-difference solution. There is no obvious difference between the two sets of theoretical curves (analytic *vs* finite-difference). The analytic function is calculated more quickly, especially for longer times in the sedimentation process. It instantly generates the corresponding concentration profile, whereas the finite-difference solver needs to start at the beginning and iterate over time steps. The analytic solution perfectly preserves the total mass in the system, whereas the finite-difference scheme causes a small increase in the total mass.[4]

VIII. CONCLUSION

It is not an entirely trivial task to evaluate numerically the analytic solution to the Mason-Weaver equation. Straightforward evaluation of the ISS by simply including a great number of terms does not always lead to satisfactory solutions, due to higher terms being evaluated as strictly zero by the floating-point arithmetic. In the original paper by M&W,[2] alternative approximate solutions were suggested that can be applied to circumvent this problem (hiPe) or significantly alleviate the computational burden (IntS). Implemented in a Python computer program,[7] the combination of these different solutions, each being operational in a specific range of parameters, leads to a computationally robust and efficient method for calculating nanoparticle sedimentation profiles.

IX. ACKNOWLEDGEMENTS

We thank Prof. Steven Abbott for his enthusiastic and eloquent communications about colloid science. Our correspondence with Prof. Abbott about solving the Mason-Weaver equation was a source of motivation for the present work.

We thank Dr Rozenn Texier-Picard (*département mathématiques*, ENS Rennes) for insightful and stimulating discussions.

[1] Seishi Shimizu and Nobuyuki Matubayasi, "Thermodynamic Stability Condition Can Judge Whether a Nanoparticle Dispersion Can Be Considered a Solution in a Single Phase.", *J. Coll. Interf. Sci.* **2020**, 575, 472.

[2] Max Mason and Warren Weaver, "The Settling of Small Particles in a Fluid", *Phys. Rev.* **1924**, *23*, 412.

[3] Colleen M. Alexander, James C. Dabrowiak, and Jerry Goodisman, "Gravitational Sedimentation of Gold Nanoparticles", *J. Coll. Interf. Sci.* **2013**, *396*, 53.

[4] Johanna Midelet, Afaf H. El-Sagheer, Tom Brown, Antonios G. Kanaras, and Martinus H. V. Werts, "The Sedimentation of Colloidal Nanoparticles in Solution and Its Study Using Quantitative Digital Photography", *Part. Part. Syst. Charact.* **2017**, *34*, 1700095.

[5] Brian D. Holt, Anne M. Arnold, and Stefanie A. Sydlik, "The Blanket Effect: How Turning the World Upside Down Reveals the Nature of Graphene Oxide Cytocompatibility", *Adv. Healthcare Mater.* **2021**, *10*, 2001761.

[6] K. E. Van Holde and R. L. Baldwin, "Rapid attainment of Sedimentation Equilibrium", *J. Phys. Chem.* **1958**, *62*, 734.

[7] Lancelot Barthe and Martinus H. V. Werts, "MasonWeaver-analytic", *Zenodo* **2022**, 7358229. doi:10.5281/zenodo.7358229

[8] Travis E. Oliphant, "Python for Scientific Computing", *Comp. Sci. Eng.* **2007**, *9*, 10.

[9] Charles R. Harris *et al.*, "Array Programming with NumPy", *Nature* **2020**, *585*, 357.

[10] Pauli Virtanen *et al.*, "SciPy 1.0: Fundamental Algorithms for Scientific Computing in Python", *Nature Methods* **2020**, *17*, 261.

[11] Mark Mitchell *et al.*, "engauge-digitizer", *Zenodo* **2020**, 3941227. doi:10.5281/zenodo.3941227